Combined experimental and kinetic modeling study of the bi-modal NO$_x$ conversion profile on commercial Cu-SAPO-34 catalyst under standard SCR conditions

Saurabh Y. Joshi[*], Ashok Kumar, Jinyong Luo, Krishna Kamasamudram, Neal W. Currier, Aleksey Yezerets[**]

Corporate Research and Technology, Cummins Inc., 1900 McKinley Avenue, Columbus, IN 47201, USA

ABSTRACT

Bi-modal NO$_x$ conversion profile has been consistently reported for selective catalytic reduction (SCR) of NO$_x$ with NH$_3$ on certain Cu-exchanged zeolite catalysts under the so-called standard SCR conditions, with two distinct NO$_x$ conversion peaks located around 250 and 450 °C. However, the nature of this practically important phenomenon remained unexplained. In this work, we have used a combination of experimental studies and kinetic modeling to characterize and de-convolute several side reactions, allowing us to quantitatively reconstruct the overall bi-modal conversion profile. In particular, we have shown that the first peak can be represented as a competition between the standard SCR reaction and parasitic NH$_3$ oxidation. The subsequent increase in the NO$_x$ conversion can be attributed to the onset of *in-situ* NO oxidation to NO$_2$ that enhances NO$_x$ reduction via fast SCR reaction route. Specifically, our modeling study indicates that NO oxidation reaction accelerates by orders of magnitude under the standard SCR conditions and becomes the governing step for NO reduction at high temperature.

© 2014 Elsevier B.V. All rights reserved.

1. Introduction

Selective catalytic reduction of NO$_x$ with ammonia (commonly referred to as NH$_3$-SCR or just SCR) has emerged as the technology of choice to meet stringent emission requirements for a variety of diesel applications worldwide. The most widely used class of NH$_3$-SCR catalysts in the USA are based on metal exchanged zeolites, especially those exchanged with Fe or Cu. The commercial NH$_3$-SCR catalysts have undergone significant advancements leading to improved stability and performance [1].

SCR process can proceed via three distinct kinetic mechanisms, depending on the ratio of NO and NO$_2$ in the total NO$_x$. According to the well-established nomenclature, when NO$_x$ is represented by NO alone (NO$_2$/NO$_x$ = 0), the process is commonly referred to as "standard" SCR reaction; with an equimolar mixture of NO and NO$_2$ (NO$_2$/NO$_x$ = 0.5), it is referred to as "fast" SCR; and finally with NO$_2$ alone (NO$_2$/NO$_x$ = 1), it is called "slow" or "NO$_2$$^-$" SCR [2].

Various aspects of catalytic behavior of commercial NH$_3$-SCR catalysts have been extensively studied in the literature. Interestingly, multiple authors have reported that certain Cu-zeolite catalysts showed characteristic behavior, where the NO$_x$ conversion profile under standard SCR conditions exhibited two peaks, as illustrated in Fig. 1a. In particular, Ma et al. [3] compared the performance of commercial Cu-SSZ-13 and Cu-SAPO-34 catalysts and reported that the catalytic activity of Cu-SSZ-13 showed a single maximum, whereas the NO$_x$ conversion profile over the Cu-SAPO-34 showed two peaks. The authors proposed that the gas-phase NO$_2$ is an important intermediate in the NH$_3$-SCR reaction at high temperatures. They showed that Cu-SAPO-34 retained many surface nitrate species and did not produce much more gas-phase NO$_2$ than Cu-SSZ-13; hindering the SCR reaction at 390 °C. Other authors [1,4] reported similar characteristic bi-modal NO$_x$ conversion profile for Cu-zeolite catalysts under standard SCR conditions. Gao et al. [5] reported in their supplementary data that the NO$_x$ conversion exhibited a bi-modal profile, with a minimum around 350 °C for the case of low ion-exchanged Cu-SSZ-13 catalyst at high space velocity. To date, none of the literature studies were able to quantitatively explain and predict this characteristic bi-modal behavior.

The primary objective of this work was to apply a combination of experimental studies and kinetic modeling to provide insights

* Corresponding author. Tel.: +1 812 377 6561.
** Corresponding author. Tel: +1 812 377 9587.
E-mail addresses: Saurabh.Joshi@cummins.com, syjoshi@gmail.com (S.Y. Joshi), aleksey.yezerets@cummins.com (A. Yezerets).

Nomenclature

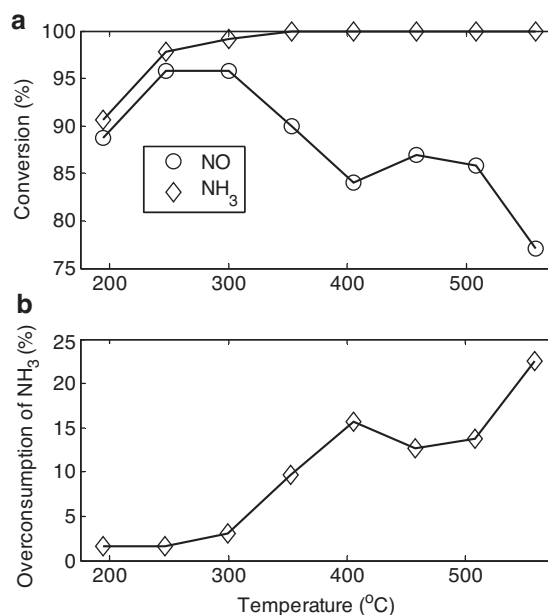|	
A_i	pre-exponential factor for reaction i $(\text{mol/m}^3_{\text{washcoat}}s)$
$C_{\text{fm},j}$	cup-mixing concentration of species j in gas phase (mol/m^3)
$C_{s,j}$	concentration of species j in washcoat (mol/m^3)
C_{pw}	specific heat capacity of solid (J/kg/K)
D_f	diffusivity of species in bulk gas phase (m^2/s)
D_{wc}	diffusivity of species in washcoat (m^2/s)
D_{Hf}	hydraulic diameter of open flow area (m)
E_i	activation energy for reaction i (J/mol)
j	species (NH_3, NO, NO_2)
k_i	rate constant for reaction i $(\text{mol/m}^3_{\text{washcoat}}s)$
k_{me}	bulk mass transfer coefficient
Nu	dimensionless heat transfer coefficient
R_i	rate of reaction i $(\text{mol/m}^3_{\text{washcoat}}s)$
$\bar{u}$	average gas velocity in the channel (m/s)
T_f	gas phase temperature (K)
T_s	temperature of washcoat/subrate (K)
t	time (s)
y_j	mole fraction of species j in gas phase
$y_{s,j}$	mole fraction of species j at gas−washcoat interface
x	coordinate in radial direction in the washcoat
z	axial coordinate

Greek letters

α_f (α_w)	thermal diffusivity of gas (solid)
ε_{wc}	void fraction of washcoat
δ_{wc}	washcoat thickness = A_{wc}/P_Ω = (cross-sectional area of washcoat/wetted perimeter) (m)
ν_{ij}	stoichiometric coefficient of species j in reaction i
Ω_1 (Ω_2)	site density of weak (strong) site (moles of NH_3/m^3 washcoat)
γ_1 and γ_2	constants in Eq. (7)
$\theta_1(\theta_2)$	fractional coverage of strong (weak) sites
ρ_w	density of solid (kg/m^3)

Fig. 1. NH_3-SCR experiments on commercial Cu-SAPO-34 SCR catalyst sample under the standard SCR conditions with feed consisting of 220 ppm of NO and 220 ppm of NH_3 along with basic components of exhaust gas (10% O_2, 8% CO_2, 7% H_2O and balance of N_2). (a) steady-state NO and NH_3 conversions as a function of catalyst temperature; (b) overconsumption of NH_3 as a function of catalyst temperature.

2. Experimental

2.1. Catalyst samples

Cylindrical samples (approximately 1-inch diameter by 3-inch length and 300 cells/in^2) were cored from a commercial Cu-SAPO-34 SCR catalyst, belonging to the structural family of chabazite (CHA). Before each experiment, the samples were pretreated (de-greened) at 700 °C for 4 h in the feed gas containing 10% O_2, 8% H_2O, 7% CO_2 and balance N_2 at 40,000/h.

2.2. Reactor set-up

The bench flow reactor experimental set-up used in this work is the same as that described in detail in our earlier work [9]. The catalyst sample was wrapped in Interam® mat which was compressed between the core and the quartz reactor tube. This enabled to prevent any gas bypassing around the catalyst periphery during the experiments. The temperatures of the catalyst and gas were measured by Omega K-type thermocouples. The catalyst inlet and outlet temperatures were measured by thermocouples located 3 mm from the inlet and outlet faces, respectively. All gases were metered by MKS mass flow controllers calibrated for their respective gas species and flow range requirements. The effluent from the flow reactor was analyzed using an FT-IR spectrometer (MKS 2030 Series).

2.3. Experimental methodology

Two different test protocols were utilized in this study: transient temperature programmed desorption (TPD) experiments were carried out to quantify NH_3 storage, while the four-step protocol developed by Kamasamudram et al. [6] and shown in Fig. 2 was used to characterize a number of catalytically relevant features. Basic components of diesel exhaust gas (10% O_2, 8% CO_2, 7% H_2O and balance of N_2) were present during the entire experiment, while NO and NH_3 were switched on and off, as shown in Fig. 2.

into the nature of the aforementioned bi-modal NO_x conversion profile.

The main challenge in the kinetic modeling of the NO_x reduction is related to the presence of the side reactions, namely parasitic NH_3 oxidation, NO oxidation and direct NH_3 oxidation by oxygen. By parasitic NH_3 oxidation, we refer to over-consumption of NH_3 beyond the stoichiometric amount of converted NO_x in the presence of SCR reaction. Remarkably, this effect is observed at much lower temperatures than those required for direct oxidation of NH_3 by oxygen in the absence of NO_x. This effect has been previously reported for other catalysts, most notably for various Fe-exchanged zeolites [6,7] and proven by Nedyalkova et al. [8] via isotopic labeling experiments using ^{15}NO.

We simplified the process of kinetics determination by deconvoluting the overall NO_x reduction catalytic activity into characteristic regimes, where each regime signified the dominance of a certain reaction. Then, the kinetics of each individual reaction was determined in its characteristic regime. We utilized 1 + 1 dimensional reactor model considering bulk mass transfer and washcoat diffusion. Thus, the gas phase concentration and solid and gas temperatures were solved in axial direction only, whereas the concentration in washcoat was solved in axial and transverse (perpendicular to flow) directions. The effective washcoat diffusivity used in modeling was determined experimentally by two independent methods as described below.

Table 1
Network of reactions and the rate expressions.

Reaction	Rate expression	Eq. number
$NH_3 + S_1 \leftrightarrow NH_3 - S_1$	$R_1 = k_{f1}y_{s,NH_3}(1-\theta_1) - k_{b1}\theta_1$	(6a)
$NH_3 + S_2 \leftrightarrow NH_3 - S_2$	$R_2 = k_{f2}y_{s,NH_3}(1-\theta_2) - k_{b2}\theta_2$	(6b)
$2NH_3 - S_1 + 1.5O_2 \rightarrow N_2 + 3H_2O + 2S_1$	$R_3 = k_3\theta_1[y_{O_2}(1+\gamma_1 y_{NO})(1+\gamma_2 y_{NO_2})$	(7)
$NO + 0.5O_2 \leftrightarrow NO_2$	$R_4 = k_{4f}y_{NO}[y_{O_2}]^{0.5}$	(8)
$4NH_3 - S_1 + 4NO + O_2 \rightarrow 4N_2 + 6H_2O + 4S_1$	$R_5 = k_5\theta_1 y_{NO}$	(9)
$2NH_3 - S_1 + 2NO + 2.5O_2 \rightarrow 4NO + 3H_2O + 2S_1$	$R_6 = k_6\theta_1 y_{NO}$	(10)
$2NH_3 - S_1 + NO + NO_2 \rightarrow 2N_2 + 3H_2O + 2S_1$	$R_7 = k_7\theta_1 y_{NO}y_{NO_2}$	(11)

Unless indicated otherwise, the inlet concentrations of both NO and NH$_3$, when present, were about 200 ppm and the gas hourly space velocity was fixed at 40,000/h (standard temperature and pressure). The protocol was applied for the case of standard SCR (NO$_2$/NO$_x$ = 0) at various temperatures. The functions characterized by the protocol were NO oxidation, NO reduction, NH$_3$ storage and NH$_3$ oxidation. Duration of individual steps was varied depending on the time required to achieve the steady-state concentration of gas components.

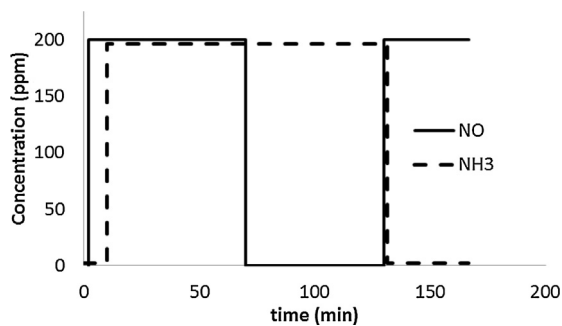## 3. Mathematical model

3.1. Reactor model

In order to develop a comprehensive mathematical model, capable of describing catalyst behavior over the practically relevant broad range of temperatures, it was necessary to address not only the kinetic characteristics of the catalyst, but the mass transfer processes as well. To determine the reaction kinetics, we have experimentally measured and incorporated such functions as NH$_3$ storage, NO oxidation, NH$_3$ oxidation and NO$_x$ reduction. For mass transfer, we have considered both bulk diffusion and internal diffusion inside catalyst washcoat layer. The latter was quantified using direct measurements of NH$_3$ diffusivity in the catalyst washcoat as described below.

The following assumptions were made while developing the model: (i) uniform radial flow distribution, so a single representative channel could be modeled; (ii) laminar flow, consistent with low Reynolds number, characteristic of such applications (typically <100); and (iii) uniform catalyst coating across the monolith. The equations used in the model were based on the study by Metkar et al. [10]. The model consists of the species balance [Eqs. (1)–(3)] and energy balance [Eqs. (4a) and (4b)].

$$\frac{\partial C_{fm,j}}{\partial t} = -\bar{u}\frac{\partial C_{fm,j}}{\partial z} - \frac{4k_{me,j}}{D_{Hf}}(C_{fm,j} - C_{s,j}) \tag{1}$$

Fig. 2. Schematic showing four-step protocol conducted on commercial Cu-SAPO-34 SCR catalyst sample under the standard SCR conditions. Feed: 200 ppm NO and NH$_3$ (when present) along with basic components of exhaust gas (10% O$_2$, 8% CO$_2$, 7% H$_2$O and balance of N$_2$).

$$\varepsilon_{wc}\frac{\partial C_{s,j}}{\partial t} = D_{wc,j}\frac{\partial^2 C_{s,j}}{\partial x^2} + \sum_i \nu_{ij}R_i \tag{2}$$

$$\Omega_k\frac{\partial \theta_k}{\partial t} = \sum \nu_j R_{\nu'} \tag{3}$$

$$\frac{\partial T_f}{\partial t} = -\bar{u}\frac{\partial T_f}{\partial z} - \frac{4\alpha_f Nu}{D_2^{Hf}}(T_f - T_s) \tag{4a}$$

$$\frac{\partial T_s}{\partial t} = \alpha_w\frac{\partial^2 T_s}{\partial z^2} + \frac{h}{\delta_w \rho_w C_{pw}}(T_f - T_s) + \frac{\delta_{wc}\sum_i R_i(-\Delta H_i)}{\delta_w \rho_w C_{pw}}. \tag{4b}$$

The subscript j represents the species (j = NH$_3$, NO, NO$_2$), $C_{fm,j}$ is cup-mixing concentration of species j in gas phase, $C_{s,j}$ concentration of species j at gas-washcoat interface. The other symbols and notations used in the above equations are elaborated in the nomenclature. The governing equations [Eqs. (1)–(4b)] were solved using commercial software, AVL BOOST$^®$ (Version 2011). We could obtain a grid-independent solution using 25 elements along the channel and 8 elements across the washcoat layer. During the transient simulations for NH$_3$-TPD, a time-step of 1 s was used.

3.2. Kinetic model

In this work, we have followed a global kinetic modeling approach based on the previously published studies [10–14]. Some of the rate expressions obtained from the literature were modified to capture our observations, as explained below.

The reactions considered and rate expressions are listed in Table 1. Arrhenius equation was used to capture temperature dependence of all the rate constants: $k_i = A_i e^{-E_i/RT}$. The kinetic parameters of individual reactions were determined in isolation by de-convoluting the overall SCR process into characteristic regimes, as described in detail below. This allowed us to minimize the number of parameters to be determined at once. Therefore, we did not require to use optimization package for parameter estimation, instead the parameters were tuned manually. The numerical values of the Arrhenius parameters are listed in Table 2.

NH$_3$ adsorption–desorption is a key step in SCR chemistry and usually the first step in kinetic modeling [11,14]. In our modeling, we considered two types of NH$_3$ adsorption sites: strong and weak [Eqs. (6a) and (6b), respectively]. The densities of these sites were obtained from NH$_3$-TPD experiment which is described in detail in Section 4.2.1. In particular, it was shown that strong sites account for approximately 88% of the total NH$_3$ adsorption sites (Table 3). Therefore, most of the NH$_3$ storage occurs on the strong sites. The weak sites comprise only a small fraction of total sites (12%) and represent physically adsorbed NH$_3$ (θ_2), which is desorbed at much lower temperatures than the strongly bound NH$_3$ (θ_1). Furthermore, it was assumed that only the strong site (θ_1) participates in the reactions and the reactions do not occur on the weak site (θ_2). We considered Temkin-type coverage dependent desorption activation energy [$E_b = E_b^0(1 - \alpha\theta_{NH_3})$], which has been used by many literature studies [10–14]. The rate expression for NH$_3$ adsorption–desorption is shown by Eqs. (6a) and (6b) in Table 1.

Table 2
Values of Arrhenius kinetic parameters used in modeling.

Reaction	k_i	A_i	Value of A_i (mol/m³ washcoat/s)	E_i	Value of E_i (kJ/mol)
NH$_3$ adsorption on site S$_1$ (R_{f1})	k_{f_1}	A_{f_1}	7.09×10^5	E_{f_1}	0
NH$_3$ desorption on site S$_1$ (R_{b1})	k_{b_1}	A_{b_1}	4.17×10^8	E_{b_1}	$70\,(1 - 0.04\theta_{NH_3})$
NH$_3$ adsorption on site S$_2$ (R_{f2})	k_{f_2}	A_{f_2}	7.09×10^5	E_{f_2}	0
NH$_3$ desorption on site S$_2$ (R_{b2})	k_{b_2}	A_{b_2}	5.57×10^7	E_{b_2}	$50\,(1 - 0.01\theta_{NH_3})$
NH$_3$ oxidation (R_3)	k_3	A_3	1.43×10^{13}	E_3	160
NO oxidation (R_4)	k_{f_4}	A_{f_4}	9.13×10^9	E_{f_4}	68
Standard SCR (R_5)	k_5	A_5	1.75×10^{12}	E_5	80
Parasitic NH$_3$ oxidation (R_6)	k_6	A_6	7.5×10^{14}	E_6	120
Fast SCR (R_7)	k_7	A_7	4.73×10^{18}	E_7	80

To model NH$_3$ oxidation, the global rate expression reported in some of the earlier literature studies [10–14] was used with some modifications. These modifications were necessary to explain the under-prediction of the ammonia oxidation rates in the presence of SCR reaction, especially at high temperatures (above 500 °C). First, the kinetics of NH$_3$ oxidation was determined directly, in the absence of NO$_x$ in the gas feed. Subsequently, it was incorporated into the overall kinetic model, where the SCR reaction kinetics was tuned at relatively low conversions, below 200 °C. But the resulting model over-predicted NO$_x$ conversion, and therefore under-predicted the rate of NH$_3$ oxidation. We attributed this discrepancy to the promotional effect of the presence of the NO$_x$ species on the ammonia oxidation reaction. This effect was empirically captured in our model by multiplying the rate expression reported in the literature [10–14], $k\theta\left[y_{O_2}\right]$ by the term: $(1 + \gamma_1 y_{NO})(1 + \gamma_2 y_{NO_2})$. Here, y_{NO} and y_{NO_2} are mole fractions of NO and NO$_2$ in the gas phase. Thus the rate expression used in this work [Eq. (7)] reduces to the literature rate expression ($k\theta\left[y_{O_2}\right]$) when NO$_x$ is absent in the feed.

The process of selective catalytic reduction of NO$_x$ with NH$_3$ is complicated by the occurrence of undesired reactions that consume NH$_3$ beyond the stoichiometric amount of converted NO$_x$. The NH$_3$ over-consumption during a typical experiment under standard SCR conditions is shown in Fig. 1b. As can be seen, the profile is non-monotonic with two distinct peaks indicating two characteristic mechanisms for the NH$_3$ over-consumption. For one of these mechanisms, NH$_3$ oxidation is prominent above 450 °C, which was discussed above and modeled using global rate expression [Eq. (7)]. We refer the other mechanism of NH$_3$ over-consumption as parasitic NH$_3$ oxidation which is observed below 400 °C. Nedyalkova et al. [8] investigated the behavior using isotope labeled ^{15}NO and showed that NH$_3$ is oxidized to form NO, but this only occurs in the presence of NO. The behavior was represented by the following global reaction in our model: NH$_3$ – S$_1$ + NO + 1.25O$_2$ → 2NO + 1.5H$_2$O + S$_1$. We derived the global rate expression for parasitic NH$_3$ oxidation [given by Eq. (10)] assuming that strongly adsorbed NH$_3$ unselectively reacted with gas-phase or weakly adsorbed NO to form two molecules of NO.

The kinetics of NO oxidation on Cu-zeolite catalyst is well studied in the literature [15,16]. We developed kinetic model for NO oxidation based on the previous studies but with some modifications. Metkar et al. [16] developed a global kinetic model for NO oxidation. Their model reduces to the following rate expression for our case of excess O$_2$ and H$_2$O.

$$R = \frac{K_1}{1 + K_2 y_{NO_2}} \left(y_{NO}[y_{O_2}]^{0.5} - \frac{y_{NO_2}}{K_{eq}} \right). \quad (5)$$

The above rate expression indicates that NO oxidation reaction is inhibited by its product NO$_2$. But Eq. (5) was obtained in the absence of SCR conditions, i.e. without NH$_3$ in the feed [16]. In this work, we quantify the rate of *in-situ* NO oxidation under standard SCR conditions and show that the *in-situ* NO oxidation is not inhibited by NO$_2$ since the NO$_2$ thus formed *in-situ* is rapidly consumed

Table 3
Values of other parameters used in modeling.

Parameter	Value	Unit
Ω_1	669.1	mol/m³ washcoat
Ω_2	90	mol/m³ washcoat
γ_1	2×10^5	[–]
γ_2	2×10^5	[–]

via fast SCR route. This implies that $y_{NO_2} \to 0$. Moreover, the rate of forward reaction is much higher than backward reaction due to rapid removal of the strong inhibitor, NO$_2$ (which implies that $k_f \gg k_b \therefore K_{eq} \gg 1$). These observations are discussed and validated in detail in Section 4.2.3.3. Thus, under standard SCR conditions, Eq. (5) can be simplified to the following equation by substituting $y_{NO_2} \to 0$ and $K_{eq} \gg 1$.

$$R_4 = k_{4f} y_{NO}[y_{O_2}]^{0.5}. \quad (8)$$

This rate expression [Eq. (8)] was used to model *in-situ* NO oxidation under standard SCR conditions.

The rate expressions for standard and fast SCR reactions [Eqs. (9) and (11)] were based on the previous work [11] assuming strongly adsorbed NH$_3$ reacts with gas-phase or weakly adsorbed NO$_x$. The slow SCR reaction (with NO$_2$ as the dominant NO$_x$ species) was not considered since the main objective of this work was to model the characteristic bi-modal behavior observed under standard SCR conditions. Moreover, the catalyst produced minimal N$_2$O (<1%) under the standard SCR conditions. So N$_2$O formation reactions were not considered in the kinetic modeling.
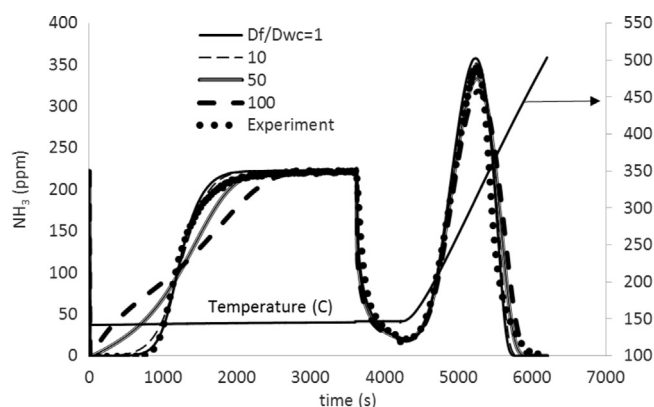
4. Results and discussion

4.1. Experimentally observed bi-modal NO$_x$ conversion profile under standard SCR conditions

Fig. 1a shows the steady-state NO and NH$_3$ conversions as a function of temperature under the standard SCR conditions (feed NO$_2$/NO$_x$ = 0). The NH$_3$ conversion increased monotonically with temperature and finally reached 100% above 300 °C. However, it is interesting to note that the NO conversion in the same experiments showed two peaks with a minimum around 400 °C. The NH$_3$ overconsumption, calculated as the difference between NH$_3$ conversion and NO conversion, is plotted in Fig. 1b. As can be seen, the profile is non-monotonic, with two characteristic slopes indicating that there are two distinct mechanisms for NH$_3$ overconsumption.

4.2. Kinetic modeling to reconstruct the bi-modal NO$_x$ conversion profile

In the following subsections, we review individual reactions and mass transfer steps and their contribution to the overall bi-modal profile.

Fig. 3. NH_3 evolution with time during the temperature programmed desorption study. Feed NH_3 = 225 ppm along with other components of exhaust gas (8% CO_2, 7% H_2O and balance of N_2). The catalyst temperature is plotted on the secondary axis.

Fig. 4. Steady-state NH_3 conversion as a function of temperature during NH_3 oxidation reaction. Feed: 220 ppm of NH_3 along with basic components of exhaust gas (10% O_2, 8% CO_2, 7% H_2O and balance of N_2). Markers represent experimental data and curves represent simulations for various values of diffusivity ratios.
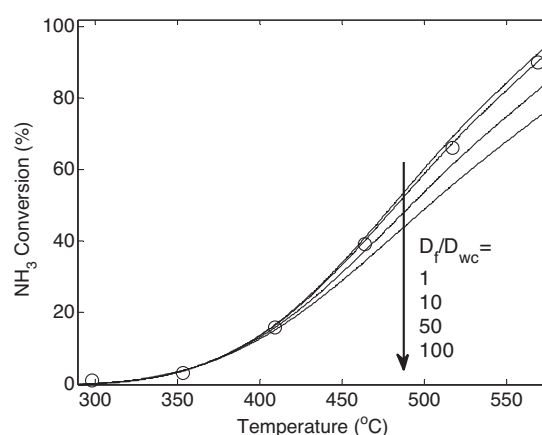
4.2.1. Ammonia adsorption–desorption and estimation of effective reactant diffusivity in the washcoat

Ammonia adsorption–desorption is a key step in the SCR chemistry and commonly the first step in kinetic modeling [11]. Temperature-programmed desorption (TPD) protocol was used to determine the kinetics of adsorption–desorption. First, the catalyst was saturated by flowing 225 ppm NH_3 for sufficient duration (~1 h) at 150 °C. Then, NH_3 feed was shut off for 10 min maintaining the same temperature (150 °C) to remove any weakly stored NH_3. The site density of weak sites (Ω_2) was determined using the amount of weakly bound NH_3 desorbed during this isothermal step. Finally, temperature was ramped to 550 °C at 11 °C/min and all the remaining NH_3 was desorbed. The amount of NH_3 evolved during this temperature ramp was used to determine the site density of strong sites (Ω_1).

Now, we elaborate a method to estimate the effective diffusivity (D_{wc}) of NH_3 in the washcoat using the experimental data for ammonia adsorption–desorption. This study was essential because the values reported in the literature vary over a wide range from 10^{-8} to 10^{-6} m^2/s, depending upon the method and catalyst studied. Huang et al. [17] used a value of 10^{-8} m^2/s for the pore diffusivities of NH_3 and NO in Fe-exchanged ZSM-5 catalyst. Metkar et al. [10] used values in the range of 10^{-6}–10^{-7} m^2/s for Fe-ZSM-5 and Cu-chabazite (CHA) catalysts. Colombo et al. [18] used effective diffusivities on the order of 10^{-7} m^2/s for a commercial Fe-promoted zeolite catalyst. However, there is not any generalized method available in literature to estimate the washcoat diffusivity for metal exchanged zeolite SCR catalysts.

In this work, we present two approaches for the estimation of D_{wc} based on using less kinetically complicated processes than the target SCR process, which is using the same essential reactants. The kinetics of NH_3 adsorption–desorption was determined neglecting washcoat diffusion limitations. Then the effect of washcoat diffusivity (D_{wc}) of NH_3 was studied on the NH_3 evolution as shown in Fig. 3. The curves in Fig. 3 represent modeling result for various values of diffusivity ratio (D_f/D_{wc}); where D_f is diffusivity of NH_3 in bulk gas phase which was calculated using Lennard-Jones potential correlations for diffusivity of NH_3 in air. The diffusivity ratio (D_f/D_{wc}) of about 1–10 was found to fit the data well. This effective diffusivity (D_{wc}) determination is in good agreement with a separate measurement carried out using NH_3 oxidation experiment, as described in the next sub-section.

The above-mentioned literature studies [10,17,18] report the diffusivity ratio in the range of 50–200 which is higher than that observed in this work. We attribute this to the difference in washcoat porosity and crystal size. In other words, the catalyst performance in this work did have weaker diffusional limitations than

the literature studies [10,17,18] due to higher washcoat diffusivity. Nevertheless, the two methods presented in this work can be utilized to determine effective diffusivity in any zeolitic washcoat.

The kinetics of NH_3 adsorption–desorption thus derived (and described in Table 2) was kept constant throughout the subsequent steps of modeling. Given the foundational nature of this kinetics, its robustness was further verified by conducting TPD experiments following different isothermal dwell times and using different ramp rates and ascertaining that the developed kinetics works for all those cases.

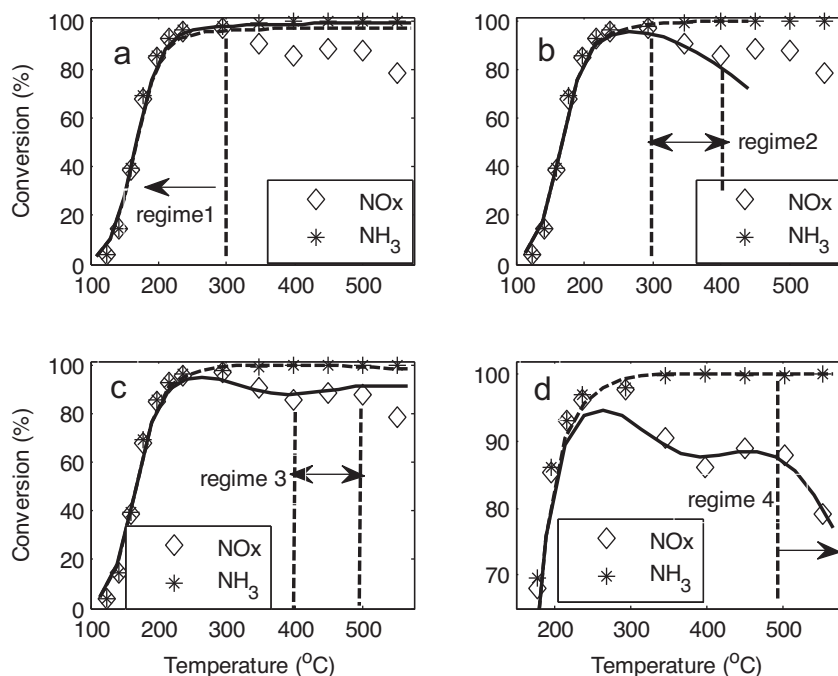### 4.2.2. NH$_3$ oxidation and estimation of the effective reactant diffusivity in the washcoat

NH_3 oxidation experiment was carried out with feed consisting of 220 ppm of NH_3 along with basic components of exhaust gas. The markers in Fig. 4 show experimental results for steady-state NH_3 conversion in the reaction of its oxidation by oxygen. The activation energy for NH_3 oxidation was determined to be 160 kJ/mol which is in excellent agreement with the value reported by Olsson et al. [11] (162.4 ± 0.05 kJ/mol). NH_3 conversions reported here are lower than the values reported in literature [10,11] for Cu-zeolite catalysts which indicates that the catalyst used in this work has lower activity for NH_3 oxidation.

Further, we utilized the NH_3 conversion data to estimate the effective washcoat diffusivity (D_{wc}) of NH_3. In particular, the data at lower conversions were utilized to determine the kinetics, while the data at higher conversions were used to tune the washcoat diffusion. As can be seen from Fig. 4, the diffusivity ratio (D_f/D_{wc}) of 10 was found to fit the data well which is in excellent agreement with the estimation from NH_3 adsorption–desorption experiment described above. Since the molecular dimensions of the reacting species (NH_3, NO and O_2) are similar; this value of diffusivity ratio (D_f/D_{wc} = 10) was used for all the reactants in all the simulations.

4.2.3. De-convoluting the NO$_x$ reduction process into four characteristic regimes

In the following subsections, we illustrate the approach of deconvoluting the NO$_x$ reduction process into four characteristic regimes, where each regime signifies dominance of a certain reaction.

4.2.3.1. Regime-1: prevalence of standard SCR reaction.
Fig. 5a–d shows steady-state conversions of NO$_x$ and NH_3 as a function of temperature under the standard SCR conditions. Fig. 5a shows regime-1 which signifies the prevalence of standard SCR reaction.

Fig. 5. Steady-state NO_x and NH_3 conversions as a function of temperature under the standard SCR conditions. Feed: 195 ppm of NO and 199 ppm of NH_3 along with basic components of exhaust gas (10% O_2, 8% CO_2, 7% H_2O and balance N_2). Markers represent experimental data and curves represent modeling result. (a) Regime-1: prevalence of standard SCR reaction, (b) regime-2: onset of parasitic NH_3 oxidation, (c) regime-3: onset of NO oxidation and (d) regime-4: onset of direct NH_3 oxidation by oxygen.

Since the NO_x and NH_3 conversions were identical, there was no over-consumption of NH_3. Thus, other side reactions were practically negligible in this regime and the experimental data were utilized to determine the kinetics of the standard SCR reaction as such. The activation energy was determined to be 80 kJ/mol. This value is in agreement with Metkar et al. [10] and Olsson et al. [11] who reported activation energy of 89.1 and 84.9 kJ/mol, respectively. As seen from Fig. 5a, model and experimental data agree very well below 300 °C.

However, above 300 °C the experimentally measured NO_x conversion diverged from the predictions as shown in Fig. 5a, arguably due to the occurrence of side reactions, including overconsumption of NH_3. Thus we proceeded to determine the kinetics of these side reactions occurring above 300 °C as described below. The kinetics of standard SCR determined in regime-1 was kept unchanged while determining the kinetics of the side reactions.

4.2.3.2. Regime-2: onset of parasitic NH_3 oxidation. Fig. 5b shows regime-2 where NH_3 conversion reached completion and the NO_x conversion slightly decreased. In this regime (300–400 °C), the rate of NH_3 consumption via direct oxidation by oxygen is insignificant, as measured by separate experiments in the absence of NO. As mentioned in the introduction, we refer to this NH_3 overconsumption as parasitic NH_3 oxidation where NH_3 oxidation is catalyzed by the presence of NO.

As shown in Fig. 5b, the experimental data can be modeled accurately over regimes-1 and -2 (120–400 °C) considering two reactions, namely standard SCR and parasitic NH_3 oxidation. We described parasitic NH_3 oxidation using the following global reaction; the rate expression for the same is given by Eq. (10).

$$2NH_3 + 2NO + 2.5O_2 \rightarrow 4NO + 3H_2O.$$
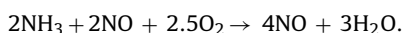
The activation energy for parasitic NH_3 oxidation was determined to be 120 kJ/mol. While determining this kinetics, the kinetics of standard SCR reaction obtained above in regime-1 was kept unchanged.

4.2.3.3. Regime-3: onset of NO oxidation. The role of NO oxidation reaction in the overall standard SCR reaction mechanism has been extensively studied and vigorously debated in the literature [11,19,20]. For example, Metkar et al. [19] proposed that this is a rate-determining step for the standard SCR reaction on Fe-zeolite catalyst, while the findings of Ruggeri et al. [20] were not supporting that argument. In this work, we present the quantitative comparison of rates of SCR reaction and *in-situ* NO oxidation under the standard SCR conditions. In particular, our modeling results show that NO oxidation reaction significantly accelerates under the standard SCR conditions and becomes the important step for NO reduction at high temperature. This enhancement in the rate of NO oxidation under the standard SCR conditions is a result of rapid removal of *in-situ* generated NO_2 via fast SCR route.

Fig. 5c shows regime-3 where NO_x conversion increased with temperature. We hypothesized that in this regime, a fraction of NO was oxidized to NO_2 *in-situ*, which was then instantaneously consumed via fast SCR reaction route. As a result, NO_x conversion slightly increased with temperature in this regime, concomitantly with the increase in the NO oxidation rate. While modeling NO_x and NH_3 conversions in this step, the kinetics of standard SCR and parasitic NH_3 oxidation obtained above in regimes-1 and 2 were kept unchanged. Also, the kinetics for fast SCR used was determined from a separate experiment (Fig. A. The difference in the NO_x and NH_3 conversions in Fig. A was due to under-stoichiometric amount of feed NH_3). It is important to note that the experimental data in regime-3 were modeled by calibrating only the NO oxidation rate expression [Eq. (8)] and activation energy was found to be 68 kJ/mol. The good agreement between model and experiment over regimes-1, -2 and -3 (120–500 °C) is evident from Fig. 5c. We show that the activation energy for NO oxidation determined in this step (68 kJ/mol) is indeed intrinsic, as elaborated below.

In order to verify our hypothesis regarding the onset of NO oxidation reaction in the regime-3, we carried out a separate set of NO oxidation experiments in the absence of SCR reaction, i.e. in the absence of NH_3 in the feed. It has been previously shown by Mulla et al. [21] that proper experimental determination of the
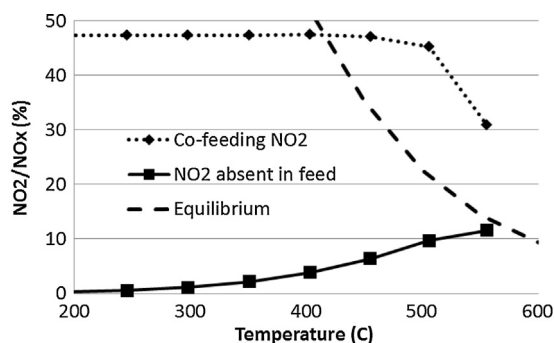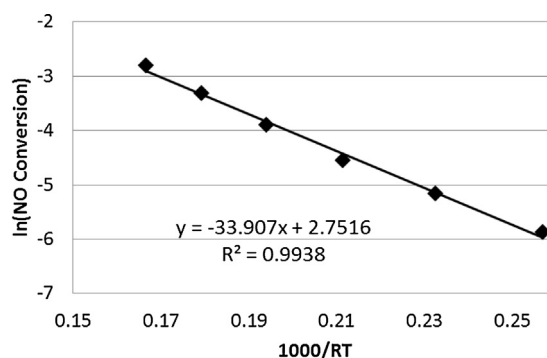
Fig. 6. Steady-state NO_2/NO_x as a function of catalyst temperature during NO oxidation experiments on commercial Cu-SAPO-34 SCR catalyst sample. Feed: (a) 95 ppm of NO_2 and 105 ppm of NO when NO_2 is co-fed, (b) 200 ppm of NO and $NO_2/NO_x = 0$ along with basic components of exhaust gas (10% O_2, 8% CO_2, 7% H_2O and balance N_2).

activation energy of the NO oxidation reaction requires presence of NO_2 in the reaction feed, for otherwise the determined value would be halved compared to the intrinsic activation energy. This is due to the inhibition of the NO oxidation process by its product.

As shown in Fig. 6 (dotted line), an attempt to measure NO oxidation properly in the presence of NO_2 was unsuccessful due to very low reaction rates under these conditions, consistent with the inhibiting role of NO_2. In fact, when NO_2 was co-fed in the reactor along with NO, virtually no oxidation was observed over the entire range where this reaction was thermodynamically favorable (area to the left of the dashed line). This is in agreement with the findings of Metkar et al. [16] who showed that a similar Cu-exchanged zeolite catalyst exhibited no measurable NO oxidation activity in the presence of NO_2.

As an alternative approach, we have measured NO oxidation in the absence of NO_2 in the feed (Fig. 6, solid line), with the expectation that the resulting activation energy would be half of the intrinsic value. Fig. 7 shows the Arrhenius plot constructed using the NO conversion data from Fig. 6 for the case of feed without NO_2. Furthermore, the NO conversion data used were in differential regime (conversion less than 10%) and were far from equilibrium. In the differential conversion regime, the turnover rate (TOR) is proportional to conversion, so ln(TOR) can be replaced by ln(conversion) to determine activation energy (Fig. 7). The apparent activation energy was found to be 33.9 kJ/mol which should correspond to the intrinsic activation energy of ~68 kJ/mol due to inhibiting effect of NO_2, as discussed above. Thus the intrinsic activation energy of the NO oxidation process

Fig. A. Steady-state NO_x and NH_3 conversions as a function of temperature under the fast SCR conditions. Feed: 100 ppm of NO and 100 ppm of NO_2 and 185 ppm of NH_3 along with basic components of exhaust gas (10% O_2, 8% CO_2, 7% H_2O and balance N_2). Markers represent experimental data and curves represent modeling result.

determined independently of the SCR reaction was found to be closely matching the value derived from the regime-3 of the SCR process, and in reasonable agreement with the value determined by Verma et al. [15] (52 ± 5 kJ/mol) for a catalyst of a similar class.

It should be emphasized that though NO oxidation conducted in the absence of SCR conditions (i.e. absence of NH_3) is strongly inhibited by NO_2, the rate of *in-situ* NO oxidation is not inhibited by NO_2 under standard SCR conditions due to instantaneous removal of NO_2 via fast SCR route. Therefore the inferred rate of NO oxidation in the presence of SCR reaction was substantially higher than the directly measured rate of NO oxidation in the absence of the SCR reaction. The ratio of the two reaction rates is shown in Fig. 8. As expected, the two predictions converge at low temperatures where NO_2 is not removed rapidly from the surface by the SCR reaction.

4.2.3.4. Regime-4: onset of direct NH_3 oxidation by oxygen. Finally, we attribute the decline of NO_x conversion in regime-4 to the onset of direct NH_3 oxidation by oxygen, as shown in Fig. 5d. To model NH_3 and NO_x conversions in this regime, we incorporated the kinetics of direct NH_3 oxidation determined in Section 4.2.2 into the overall kinetic model, where the kinetics determined in regimes-1, -2 and -3 were kept unchanged. But the resulting NO_x conversion was over-predicted, indicating under-prediction of NH_3 oxidation rate. We attributed this discrepancy to the enhancement of rate of NH_3 oxidation under SCR conditions. This enhancement factor $(1 + \gamma_1 y_{NO})(1 + \gamma_2 y_{NO_2})$ is shown in Eq. (7). The coefficient, γ_1 was determined by fitting the data in regime-4, where the kinetics determined in regimes-1, -2 and -3 and the kinetics of direct NH_3 oxidation from Section 4.2.2 were kept unchanged. γ_2 was determined by fitting the high temperature (>500 °C) data for fast SCR reaction from Fig. A in the appendix. The good agreement between the model and experimental data is evident from Fig. 5d; the plot is zoomed in to magnify the characteristic two peaks in NO_x conversion.
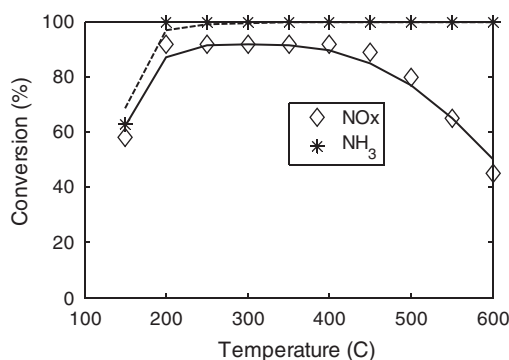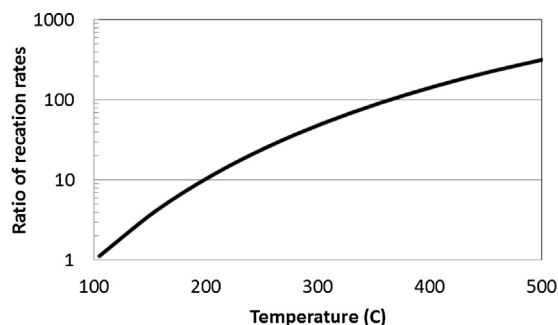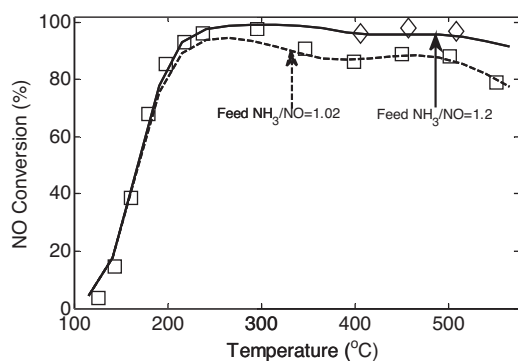

Fig. 7. Determination of apparent activation energy for NO oxidation on commercial Cu-SAPO-34 SCR catalyst assuming differential conditions. Feed: 200 ppm of NO ($NO_2/NO_x = 0$) along with basic components of exhaust gas.

Fig. 8. Ratio of simulated reaction rates of *in-situ* NO oxidation under standard SCR conditions and NO oxidation in absence of SCR conditions.

Fig. 9. Steady-state NO conversions for different NH_3/NO in feed. Feed: 195 ppm of NO and 199 (and 234) ppm of NH_3 along with basic components of exhaust gas (10% O_2, 8% CO_2, 7% H_2O and balance N_2). Markers represent experimental data and curves represent modeling result.

5. Discussion

As shown above, we were able to reconcile the bi-modal NO_x conversion profile over a commercial Cu-SAPO-34 catalyst based on a superposition of several reactions such as standard SCR, parasitic NH_3 oxidation, NO oxidation enabling fast SCR and direct NH_3 oxidation. While this mathematical formalism allowed us to describe the target behavior over the entire range of temperatures, it does not preclude the possibility of other explanations. In this section, we have considered this formalism from several standpoints, including its physical viability, some of its experimentally verifiable consequences and the possibility of alternative explanations.

The proposed formalism hinges on the assumption that two of the underlying reactions are greatly accelerated under the SCR conditions compared to the SCR-independent measurements. This includes parasitic NH_3 oxidation and NO oxidation. This possibility is underpinned by the in-operando XAS studies reported by McEwen et al. [22] which showed that the concerted presence of NO and NH_3 over a catalyst of the same class drastically promoted the overall redox activity of the Cu sites.

As discussed above, the decline in NO_x conversion with temperature observed in regime-2 can be reconciled based on the over-consumption of NH_3 in the presence of SCR reaction. One logical consequence of this hypothesis is that the limitation can be resolved by feeding over-stoichiometric amounts of NH_3. Indeed, this was experimentally confirmed as shown in Fig. 9. It may be instructive to de-convolute the contribution of various individual reactions of the above experimental results by a superposition of their calculated rates, as shown in Fig. 10. For the purposes of this comparison, we chose to plot these calculated reaction rates at 10% of the catalyst length, corresponding to the local space velocity of 400,000/h. As can be seen in Fig. 10, standard SCR reaction is dominant below 350 °C. Parasitic NH_3 oxidation reaction becomes important above 350 °C, which consumes excess NH_3 so the standard SCR reaction rate decreases sharply due to the deficit of NH_3 (Fig. 10). Therefore feeding an over-stoichiometric amount of NH_3 partially resolves this deficit, thus increasing the rate of standard SCR above 350 °C (Fig. 10b). The onset of NO oxidation reaction occurs above 350 °C generating in-situ NO_2, which is consumed instantaneously by the fast SCR reaction. The NO oxidation forward reaction is accelerated by orders of magnitude at this temperature due to the removal of NO_2 which is a strong inhibitor. In fact, the rate of NO oxidation is the highest above 450 °C and it becomes the rate-determining step for NO reduction above 450 °C. As expected, the rates of NO oxidation and fast SCR are identical initially since fast SCR is limited by the availability
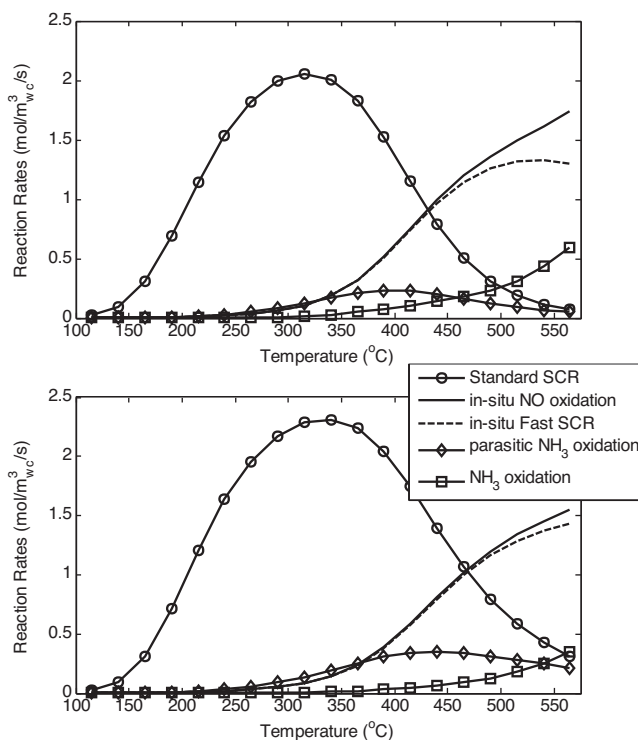
Fig. 10. Calculated rates of various reactions under standard SCR conditions. The reaction rates are function of position along length. The plot shows simulated reaction rates at 10% length (where local S.V. is 400,000/h). (a) NH_3/NO in feed is 1.02. Feed: 195 ppm of NO and 199 ppm of NH_3 (b) NH_3/NO in feed is 1.2. Feed: 195 ppm of NO and 234 ppm of NH_3.

of the in-situ-generated NO_2. Though fast SCR reaction occurs over a broad temperature range for equimolar NO and NO_2 in the feed (Fig. A), the in-situ fast SCR under standard SCR conditions is prominent above 350 °C because it is limited by the availability of the in-situ-generated NO_2. Finally, direct NH_3 oxidation by O_2 reaction becomes important above 500 °C.

Considering the possible alternative explanations, it is important to mention that Gao et al. [5] reported bi-modal NO_x conversion profile for a catalyst of a similar class, without any NH_3 overconsumption in the temperature range corresponding to regime-2. This implies that the formalism proposed in this work which relies on NH_3 over-consumption to explain the decline in NO_x conversion in regime-2 may not be universal. Several alternative formalisms can be advanced to explain this behavior. One of these includes rapid desorption of ammonia from the catalyst with temperature, outpacing the increase in the intrinsic SCR reaction rate. Another explanation may involve certain changes in the nature of the active sites with temperature [23].

6. Conclusions

In this work, we developed a kinetic model quantitatively describing an unusual phenomenon related to the bi-modal NO_x conversion profile versus temperature for certain Cu-exchanged zeolite catalysts. This behavior was represented by a superposition of four different processes with different regions of dominance including standard SCR reaction, parasitic oxidation of NH_3, NO oxidation enabling fast SCR reaction and finally direct NH_3 oxidation. This attribution allowed us to model each reaction independently of others.

The developed formalism hinges on the hypothesis that the redox activity of the catalyst is significantly enhanced under the

SCR conditions, owing to the joint presence of NO and NH_3. This is consistent with the experimental findings by McEwen et al. [22] regarding the remarkable concerted effect of these two species on the redox behavior of Cu sites in the zeolite catalysts of the same family. Consequently, the inferred rate of parasitic NH_3 oxidation under SCR conditions was found to be substantially higher than the values measured directly in the absence of NO. This hypothesis was strengthened by the additional experimental data, showing that over-stoichiometric supply of NH_3 can overcome the reactant deficit caused by the over-consumption.

Our modeling study showed that *in-situ* NO oxidation was not inhibited by NO_2 under the standard SCR conditions, since the NO_2 species generated *in-situ* were instantaneously consumed by the fast SCR reaction. As a result, the forward rate of *in-situ* NO oxidation accelerated by orders of magnitude and finally it became the important step in NO reduction at high temperature.

In addition, the related mass transfer processes, including bulk and internal washcoat diffusion, were incorporated into the model. We proposed two methods to determine washcoat diffusivity using NH_3-TPD and NH_3 oxidation experiments. The washcoat diffusivity estimated by these two methods agreed very well.

The proposed mechanism reconciles the entire range of experimental observations for this catalyst; however, it does not preclude the possibility of other explanations, especially for other catalysts where the over-consumption of NH_3 is not as pronounced.

Acknowledgements

References

[1] J.M. Fedeyko, H. Chen, T.H. Ballinger, E.C. Weigert, H. Chang, J.P. Cox, P.J. Andersen, SAE Paper (2009), 2009-01-0899.
[2] M. Colombo, I. Nova, E. Tronconi, Catal. Today 197 (2012) 243–255.
[3] L. Ma, Y. Cheng, G. Cavataio, R.W. McCabe, L. Fu, J. Li, Appl. Catal. B: Environ. 156–157 (2014) 428–437.
[4] J. Girard, R. Snow, G. Cavataio, C. Lambert, SAE Paper (2007), 2007-01-1581.
[5] F. Gao, E.D. Walter, E.M. Karp, J. Luo, R.G. Tonkyn, J.H. Kwak, J. Szanyi, C.H.F. Peden, J. Catal. 300 (2013) 20–29.
[6] K. Kamasamudram, N.W. Currier, A. Yezerets, Catal. Today 151 (2010) 212–222.
[7] V. Bacher, C. Perbandt, M. Schwefer, R. Siefert, S. Pinnow, T. Turek, Appl. Catal. B: Environ. 162 (2015) 158–166.
[8] R. Nedyalkova, K. Kamasamudram, N.W. Currier, J. Li, A. Yezerets, L. Olsson, J. Catal. 299 (2013) 101–108.
[9] C. Henry, K. Kamasamudram, N. Currier, A. Yezerets, M. Castagnola, H. Chen, SAE Paper (2012), 2012-01-1084.
[10] P. Metkar, M. Harold, V. Balakotaiah, Chem. Eng. Sci. 87 (2013) 51–66.
[11] L. Olsson, H. Sjovall, R.J. Blint, Appl. Catal. B: Environ. 81 (2008) 203–217.
[12] C. Ciardelli, I. Nova, E. Tronconi, B. Konrad, D. Chatterjee, K. Ecke, M. Weibel, Chem. Eng. Sci. 59 (2004) 5301–5309.
[13] D. Chatterjee, T. Burkhardt, M. Weibel, I. Nova, A. Grossale, E. Tronconi, SAE Paper (2007), 2007-01-1136.
[14] E. Tronconi, I. Nova, C. Ciardelli, D. Chatterjee, B. Bandl-Konrad, T. Burkhardt, Catal. Today 105 (2005) 529–536.
[15] A.A. Verma, S.A. Bates, T. Anggara, C. Paolucci, A.A. Parekh, K. Kamasamudram, A. Yezerets, J.T. Miller, W.N. Delgass, W.F. Schneider, F.H. Ribeiro, J. Catal. 312 (2014) 179–190.
[16] P.S. Metkar, V. Balakotaiah, M.P. Harold, Catal. Today 184 (2012) 115–128.
[17] H.Y. Huang, R.Q. Long, R.T. Yang, Appl. Catal. A: General 235 (2002) 241–251.
[18] M. Colombo, I. Nova, E. Tronconi, V. Schmeißer, B. Bandl-Konrad, L. Zimmermann, Appl. Catal. B: Environ. (2012) 111–112, 106-118.
[19] P.S. Metkar, N. Salazar, R. Muncrief, V. Balakotaiah, M.P. Harold, Appl. Catal. B: Environ. 104 (2011) 110–126.
[20] M.P. Ruggeri, I. Nova, E. Tronconi, Top. Catal. 56 (2013) 109–113.
[21] S.S. Mulla, N. Chen, W.N. Delgass, W.S. Epling, F.H. Ribeiro, Catal. Lett. 100 (2005) 267–270.
[22] J.S. McEwen, T. Anggara, W.F. Schneider, V.F. Kispersky, J.T. Miller, W.N. Delgass, F.H. Ribeiro, Catal. Today 184 (2012) 129–144.
[23] J.H. Kwak, T. Varga, C.H.F. Peden, F. Gao, J.C. Hanson, J. Szanyi, J. Catal. 314 (2014) 83–93.